ELSEVIER

Journal of Structural Geology 26 (2004) 2285–2295

JOURNAL OF STRUCTURAL GEOLOGY

www.elsevier.com/locate/jsg

K–Ar dating of fault gouge in the northern Sydney Basin, NSW, Australia—implications for the breakup of Gondwana

H. Zwingmann[a,b,*], R. Offler[c], T. Wilson[c], S.F. Cox[d]

[a]*CSIRO—Division of Petroleum Resources, PO Box 1130, Perth, 6102, Australia*
[b]*John deLaeter Centre of Mass Spectrometry—School of Applied Geology, Curtin University, WA 6102, Australia*
[c]*Discipline of Earth Sciences, School of Environmental and Life Sciences, University of Newcastle, Callaghan, NSW 2308, Australia*
[d]*Department of Earth and Marine Sciences and Research School of Earth Sciences, The Australian National University, Canberra, ACT 0200, Australia*

Received 14 March 2003; received in revised form 31 March 2004; accepted 31 March 2004

Abstract

The occurrence of synkinematic and authigenic clay minerals is a common feature in fault gouges. Few attempts have been made to date fault gouges. We present the first age data in Australia for synkinematic illite–smectite growth in two fault zones of the northern Sydney Basin, NSW. The faults occur at Burwood Beach, NSW in the northern part of the Sydney Basin and are hosted by Early Permian siltstones, tuffs and coals of the Lambton Formation, Newcastle Coal Measures. The faults are 1.5 m apart, show normal displacement and trend N–S with steep easterly dips. Foliated gouge zones, comminution and dilational breccias are developed along both fault surfaces. K–Ar ages extracted from samples in the gouge and tuffs in the damage zones are 172 (6–10 μm) to 119 Ma (<0.4 μm), respectively. Older ages of 272–281 Ma for the coarse fractions (>2 μm), 237–245 Ma for the <2 μm fraction, 218 Ma for the <0.4 μm fraction and 196 Ma for the <0.1 μm fraction have been obtained from siltstones within and outside the damage zone. We believe the younger ages of 196–237 Ma indicate the time at which diagenetic illite–smectite formed and the 122–150 Ma dates from the <2 μm fraction represent the maximum age of gouge formation. The younger ages are thought to reflect the last slip event occurring on the faults, which is related to the rifting and dispersal of the eastern margin of the Australian continent.

Keywords: Gouge; K–Ar dating; Sydney Basin; Australia

1. Introduction

Early studies by Lyons and Snellenberg (1971) highlighted the potential of applying isotopic dating techniques to determine the absolute timing of fault movement. Subsequently, many efforts have been made to date fault movements using different isotopic methods ranging from K–Ar, Rb–Sr to Electron Spin Resonance (ESR). Recently, several studies on fault gouges focusing on the timing of fault movement by Rb–Sr and K–Ar dating have been carried out (Kralik et al., 1987; Pevear et al., 1997; Choo and Chang, 2000). Vrolijk and van der Pluijm (1999) have used K–Ar dating in combination with mineralogical and textural observations, to determine the fault processes involved in the formation of clay gouge in thrust belts. Most studies use conventional K–Ar methods to date synkinematic illite, which is K-bearing. However, in a recent study van der Pluijm et al. (2001) reported the first ^{40}Ar–^{39}Ar dating of illite in fine-grained fault gouge using a microencapsulation technique to address and monitor ^{39}Ar recoil. The aim of this paper is to present K–Ar data obtained from fault gouge and host rock in a well documented fault zone, Burwood Beach, Newcastle, New South Wales, Australia (Wilson et al., 2000). These data indicate the timing of diagenesis in the rocks hosting the fault zones and the maximum age of slip movement on the faults. Further, they constrain the earlier deformation events associated with the rifting of the eastern margin of Gondwana during the Early Cretaceous.

* Corresponding author. Tel.: +61-892664681; fax: +61-892663153
E-mail addresses: horst.zwingmann@csiro.au (H. Zwingmann), robin.offler@newcastle.edu.au (R. Offler), stephen.cox@geology.anu.edu.au (S.F. Cox).

0191-8141/$ - see front matter
doi:10.1016/j.jsg.2004.03.007

2. Geological setting

The faults examined in this study occur at Burwood Beach, ~5 km south-west of Newcastle in the northern part of the Sydney Basin, eastern Australia (Fig. 1). They are hosted by Late Permian siltstones, tuffs (Nobbys Tuff) and Nobbys and Victoria Tunnel Coals of the Lambton Formation, Newcastle Coal Measures. Faulting appears to have taken place at depths of <2 km (Diessel, pers. com.) based on the depth of overburden on top of the Newcastle Coal Measures. This depth has been calculated from a vitrinite reflectance (Ro)-depth factor obtained from the Swansea bore ~20 km south of the study area (Diessel, 1975). Further, Ro values of 0.7 obtained from coal fragments within the fault gouge suggest temperatures no greater than 110 °C existed during faulting (Barker, 1993). The faults are normal, subparallel and approximately 1.5 m apart and are the result of a protracted deformation history (Table 1). They trend N–S, have steep easterly dips and are associated with NW-trending and steep SW dipping normal faults, which are dominant in the area. A total displacement of 10 m occurred on the western fault, and 3 m on the eastern fault. They have a damage zone in which antithetic, normal and reverse faults, and bedding parallel slip surfaces occur and a core zone containing 1-cm-wide foliated gouge zones. The latter represent the regions in which the majority of slip has been accommodated. Microscopic examination of samples from these zones reveals the presence of cataclasites, ultracataclasites and foliated gouge. In some samples the foliated gouge is overprinted by relatively undeformed barite rosettes that represent growth in an interseismic interval. The rosettes are partly comminuted, suggesting slip occurred after their formation (Wilson et al., 2000).

3. Analytical methods

3.1. Sample preparation

Eleven samples of approximately 200 g of fresh material were collected from the core zones and siltstones and tuffs, within and outside the damage zone. To avoid possible contamination, samples were collected directly from the gouge zone 30 cm below the surface. This approach follows the sampling techniques recommended by Emery and Robinson (1993) for the dating of clay minerals in sandstones. Host rock samples were collected to determine the timing of diagenesis and to ascertain whether resetting of isotopic signatures had occurred during faulting. The samples were reduced to chips with maximum dimension < 10 mm by hammer and then gently disaggregated using a repetitive freezing and thawing technique to avoid artificial reduction of size of the rock components and contamination with K-bearing minerals such as K-feldspar and micas (Liewig et al., 1987). Smaller 2, 2–6, 6–10 μm fractions were separated in distilled water according to Stoke's law and the efficiency of this separation was controlled by a laser granulometer. Additional grain size fractions <0.4 and 0.1 μm were separated using a high-speed centrifuge.

3.2. K–Ar dating

Potassium content was determined by atomic absorption using Cs for ionisation suppression. Sample aliquots of 100–200 mg were dissolved with HF and HNO_3. The samples, once in solution, were diluted to 0.3–1.5 ppm K for the atomic absorption analysis. The pooled error of duplicate K determination on all samples and standards is better than 2%. K–Ar isotopic determinations were performed using a procedure similar to that described by Bonhomme et al. (1975). Samples were pre-heated under vacuum at 80 °C for several hours to reduce the amount of atmospheric Ar adsorbed onto the mineral surfaces during sample handling. Argon was extracted from the separated mineral fractions by fusing samples within a vacuum line serviced by an on-line ^{38}Ar spike pipette. The isotopic composition of the spiked Ar was measured with an on-line VG3600 mass spectrometer using a Faraday cup. The ^{38}Ar spike was calibrated against biotite GA1550 (McDougall and Roksandic, 1974). After fusion of the sample in a low blank Heine resistance furnace, the released gases were subjected to a two-stage purification procedure with a CuO getter for the first step and two Ti getters for the second step. Blanks for the

Table 1
Deformation history[a] of the rocks in the Newcastle area

(1)	Formation of NW- and NE-trending extension joints.[b]
(2)	NW-trending thrust faults and associated folding. Late Triassic Hunter thrust deformation.
(3)	NE-trending normal faults.
(4)	WNW–NW–NS-trending normal faults.[c]
(5)	N–NNE-trending thrusts and associated folding.
(6)	WNW–NW-trending thrusts and associated folding.

E–W-trending faults also occur but time relationships are not known.

[a] History based on mine scale structural observations in the Newcastle Coalfield (Lohe and McLennan, 1991; Lohe et al., 1992).

[b] Evidence for dextral strike-slip movement on these joints has been noted on wave cut platforms, Newcastle (Blayden, 1971: Offler, unpubl.) They have formed pre-78 Ma dyke.

[c] Dyke swarms are parallel to the normal fault systems and are considered to be contemporaneous. The dykes are alkali, within plate basalts (Maxwell, 1990) and have K–Ar ages of 111, 90 (whole rock; Embleton et al., 1985) and 79 Ma (plagioclase; Zwingmann, unpubl. data).

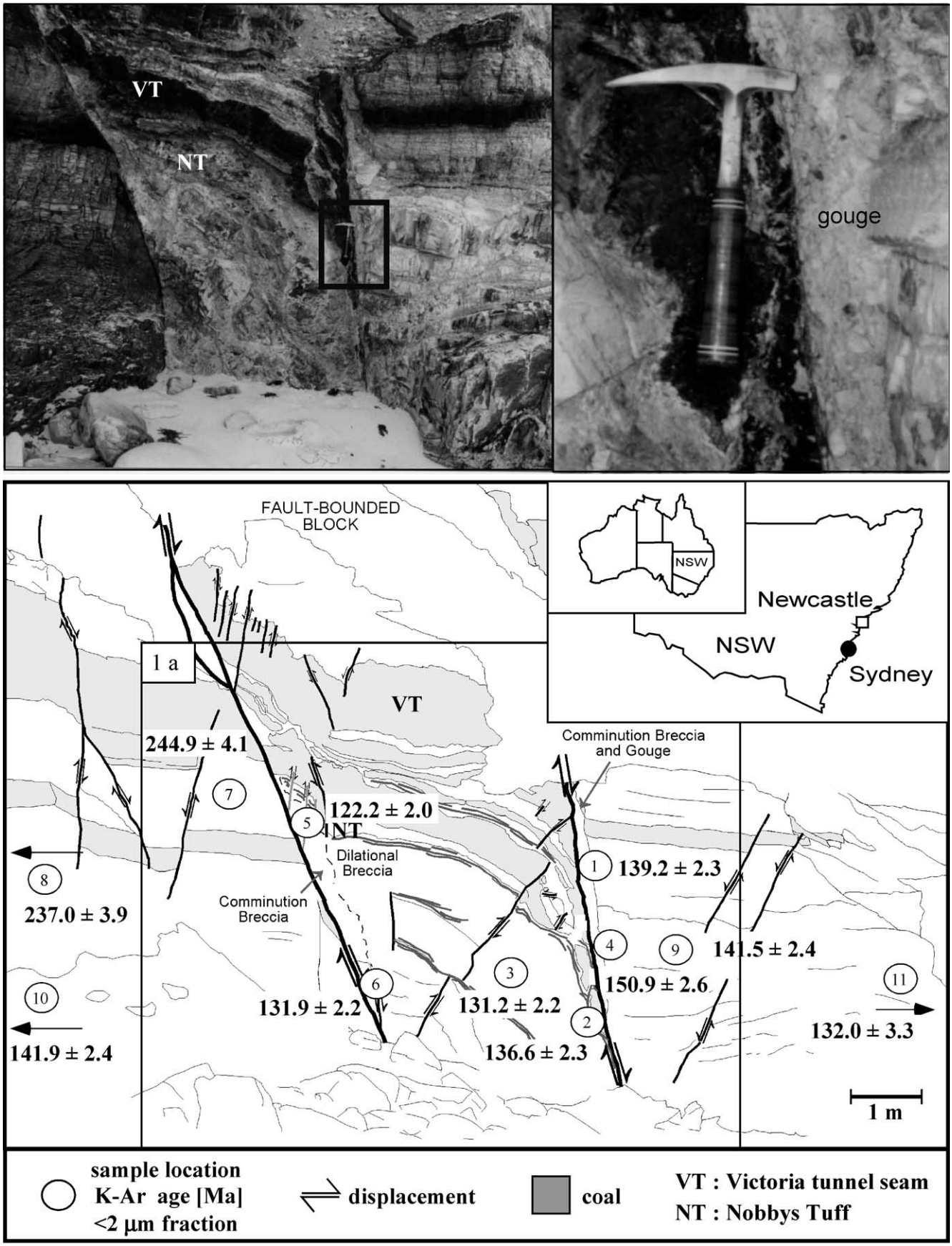

Fig. 1. (a) Photograph of normal faults at Burwood Beach. Note drag of Nobbys Tuff (NT) and Victoria Tunnel seam (VT) into fault. (b) Enlargement of inset in (a) showing comminuted coal along fault zone. (c) <2 μm K–Ar ages obtained from samples at each location. Inset: location of study area.

Table 2
K–Ar data for various fractions obtained from samples in the damage zone and fault gouge

ID Burwood Beach	Position	sample [μm]	K [%]	Rad. ^{40}Ar [mol/g]	Rad. ^{40}Ar [%]	Age [Ma]	Error [Ma]
BB1	Fault	40 <0.1	3.15	7.9200×10^{-10}	89.34	139.44	2.04
		40 <0.4	3.03	6.4676×10^{-10}	75.71	119.05	2.37
		40 <2	3.48	8.0340×10^{-10}	62.59	139.23	2.29
		40 2–6	3.09	8.6904×10^{-10}	70.82	164.45	2.92
		40 6–10	2.92	9.1591×10^{-10}	89.04	172.34	3.42
BB2	Fault	41 <2	4.05	8.9197×10^{-10}	78.56	136.75	2.29
		41 2–6	3.42	8.6620×10^{-10}	80.81	153.83	2.55
BB3	Host	42 <2	4.23	8.9487×10^{-10}	87.26	131.24	2.16
		42 2–6	3.00	7.3515×10^{-10}	92.45	145.86	2.71
BB4	Fault	43 <2	3.77	9.3639×10^{-10}	59.28	150.91	2.64
		43 2–6	2.98	8.0884×10^{-10}	67.93	159.30	2.68
BB5	Fault	44 <0.4	3.54	7.6998×10^{-10}	87.33	121.24	2.42
		44 <2	3.47	6.9704×10^{-10}	86.51	122.15	2.04
		44 2–6	2.76	6.3250×10^{-10}	89.94	138.14	2.27
		44 6–10	2.55	6.5405×10^{-10}	91.82	142.13	2.83
BB6	Fault	45 <2	2.83	6.1461×10^{-10}	89.64	131.88	2.18
		45 2–6	2.37	5.8628×10^{-10}	84.21	147.45	2.47
BB7	Host	46 <0.1	3.91	1.4113×10^{-9}	95.47	196.95	3.92
		46 <0.4	4.55	1.8295×10^{-10}	95.19	218.09	4.31
		46 <2	4.09	1.7424×10^{-9}	93.69	244.89	4.05
		46 2–6	3.21	1.5330×10^{-9}	97.82	272.04	4.46
		46 6–10	2.76	1.2395×10^{-9}	97.59	273.96	6.06
BB8	Host	47 <2	4.13	1.6828×10^{-9}	94.04	237.04	3.90
		47 2–6	3.09	1.5391×10^{-9}	98.05	281.75	4.72
BB9	Host	48<0.4	4.04	8.7623×10^{-10}	81.67	120.90	2.44
		48 <2	2.91	6.9929×10^{-10}	86.73	141.45	2.40
		48 2–6	4.06	8.4088×10^{-10}	83.94	126.82	2.12
		48 6–10	2.08	6.3360×10^{-10}	94.27	167.59	3.32
BB10	Host	49 <2	5.24	1.2242×10^{-9}	90.51	141.93	2.44
	Tuff	49 <2 D	5.24	1.2517×10^{-9}	88.76	144.99	2.42
		49 2–6	4.11	1.0535×10^{-10}	93.66	150.49	2.47
BB11	Fault	50 <2	2.32	5.0358×10^{-9}	90.72	132.00	2.33
		50 2–6	2.32	5.8050×10^{-10}	91.69	147.99	2.44

D indicates sample duplicate.

extraction line and mass spectrometer were systematically determined and the mass discrimination factor was determined periodically by airshots. Normally 20 mg of sample material was required for Argon analyses. During the course of the study, standards ($n=10$) and airshot values were measured ($n=24$). The K–Ar dating results are summarised in Table 2. The error for Argon analyses is below 1% and the ^{40}Ar/^{36}Ar value for airshots averaged 293.39 ± 0.29 (2σ, $n=24$). The K–Ar ages were calculated using ^{40}K abundance and decay constants recommended by Steiger and Jäger (1976).

3.3. X-ray diffraction

The various fractions separated from the samples were sedimented onto glass slides. Diffractograms were obtained from air-dried, glycolated and heated (550 °C) slides and analysed using a Philips automated PW1732/10 X-ray diffractometer, CuKα radiation, graphite monochrometer and 40 kV/30 mA. Samples were scanned over the range $2\theta=2$–30° at 0.02°2θ/s using divergence and scatter slits of 1° and a receiving slit of 0.2 mm. Identification of clay mineralogy and determination of the percentage of illite in illite–smectite was determined following the methods of Moore and Reynolds (1989). The percentage of $2M_1$ muscovite relative to 1 Md illite was determined from the ratio $I_{2.80\ Å}/I_{2.58\ Å}$ (Maxwell and Hower, 1967). XRD limits are around 3% and contamination phases cannot be detected below this value.

3.4. Scanning and transmission electron microscopy

Scanning electron microscope images were obtained from a PHILIPS XL30 SEM and transmission electron microscope images from a JEOL 2010 200 KV TEM. Scanning electron microscopy (SEM) was used to determine features and size of the white mica platelets exposed in samples, which had been broken approximately perpendicular to bedding. Transmission electron microscopy (TEM) was used to identify and distinguish authigenic clays from contaminants by individual grain analysis for a purity control as proposed by Hamilton et al. (1989) to detect traces of contamination phases below the XRD detection limit of 3%.

3.5. Petrographic–SEM–TEM studies

The host rocks are fine-grained siltstones, tuffs and coal. The siltstones consist of closely packed, angular grains of quartz, neoformed white mica, coalified phytoclasts and minor detrital muscovite (Fig. 2A). Bedding in these rocks is defined by oriented, wispy aggregates of coalified phytoclasts and white mica. In samples containing pelitic units or from the damage zone, illite–smectite (I/S) is more common. SEM studies reveal that the I/S crystallites in siltstones from the damage zone have a stronger preferred orientation and slightly more regular boundaries (Fig. 2B and C) than those outside. TEM analyses confirm these observations.

The tuffs consist of coarse angular fragments of quartz, less common plagioclase, K-feldspar, degraded biotite and accessory apatite, zircon and altered opaque minerals. The groundmass is dominated by oriented white mica, irregular aggregates of unoriented white mica that has replaced lithic clasts, and minor kaolinite. The ghost-like outlines of shards can be observed in some specimens. SEM studies indicate that the size of crystals in tuffs from the damage zone is greater and boundaries more regular than those in the associated siltstones. Although the Victoria Tunnel seam has not been examined in this study, analyses done by Diessel (1992) in other locations show that vitrinite is the dominant maceral and less common are liptinite, inertinite and mineral matter. Gouge samples typically show an anastamosing foliation defined by I/S wrapping around angular to subangular clasts of tuff of variable size, which are partly to completely illitised and in some cases replaced by kaolinite (Fig. 2D and E). The strong preferred orientation suggests the crystals in the gouge are of synkinematic origin. The TEM and SEM observations of the separated clay fine fractions from the gouge and host rocks indicates three distinct groups of particles: (1) idiomorphic illite fibres with elongated, sharp shapes for filamentous illite (Fig. 2F), (2) idiomorphic platy illite flakes, together with hexagonal idiomorphic kaolinite with clear sharp crystallized edges (Fig. 2C), and (3) detrital electron dense–dark particles with diffuse and irregular edges (Fig. 2C), occurring more commonly in coarser fractions (Fig. 2C). Detrital clay particles are normally volumetrically much greater than neoformed illite particles in the <2 μm and are characterized by different morphological shapes. Detrital illite normally shows irregular edges, whilst neoformed illite particles have sharp and well-defined edges (Hunziker et al., 1987; Clauer and Chaudhuri, 1995). The fibrous and platy idiomorphic shape of the illite in the tuffs outside and within the damage, and fault gouge suggest an in-situ neoformation. Their presence in the gouge supports a synkinematic origin for them.

4. Clay mineralogy

XRD analyses of samples are summarized in Table 3 and typical XRD traces are shown in Fig. 3. I/S and kaolinite are the major clay mineral components of the 2–6 μm fractions. Chlorite is an additional phase in the host rocks. Further, the XRD analyses reveal that in the 2–6 μm fraction variable contents or the $2M_1$ polytype are present (range 5–28%; mean 13; $n=11$; $\sigma n-1=6.06$). However, in the <0.5 μm fraction no $2M_1$ polytype was detected. In most fractions, I/S contains 70–90% illite suggesting temperatures ~ 100 °C during the growth of this mineral (Merriman and Kemp, 1996), which accords with temperatures of ~ 110 °C determined from vitrinite reflectance data obtained from coal in the fault gouge.

5. K–Ar data

K–Ar ages of fractions (<0.1 to 6–10 μm) separated from different host and fault rock units yield values ranging from 281 ± 5 to 119 ± 2 Ma ($n=33$; Figs. 1 and 4; Table 2). Radiogenic ^{40}Ar ranges from 98.1 to 59.3% indicating negligible atmospheric Ar contamination and reliable analytical conditions for all analyses. The reliability of the ages is also confirmed by the agreement within 2σ analytical uncertainties for duplicate analyses of <2 μm fractions of one sample (Table 2, sample BB10). The low to medium K contents for most illite fractions are consistent with a neoformed origin (see Clauer and Chaudhuri, 1995). Lower K concentration in some size fractions is caused by contamination with other mineral phases such as quartz and kaolinite identified in the XRD analysis.

6. Discussion of results

6.1. K–Ar dating of illite

For K–Ar ages of illite separates to be related to geologically meaningful events it is important that the assumptions underlying the method are carefully reviewed. The validity and importance of the assumptions involved in K–Ar dating of authigenic clays and illite (e.g. contamination, closed system behaviour, excess Ar) are discussed in detail by Hamilton et al. (1992) and Clauer and Chaudhuri (1995). The most important assumptions to consider are:

1. There is no loss or gain of either ^{40}K or ^{40}Ar after the illite has formed, i.e. closed system behaviour. This is most likely to occur during heating of the illite to a temperature where Ar may be lost by thermal diffusion. Transformation to a more thermally stable polytype may accompany the diffusion.
2. Illite of only one generation is the only K-bearing phase present in the analysed fraction, i.e. no contamination. This is a significant hurdle to the acquisition of meaningful K–Ar ages particularly in samples containing either small amounts of K-bearing detritus or a mixture of illites formed at different times. This assumption is rarely fulfilled within sedimentary

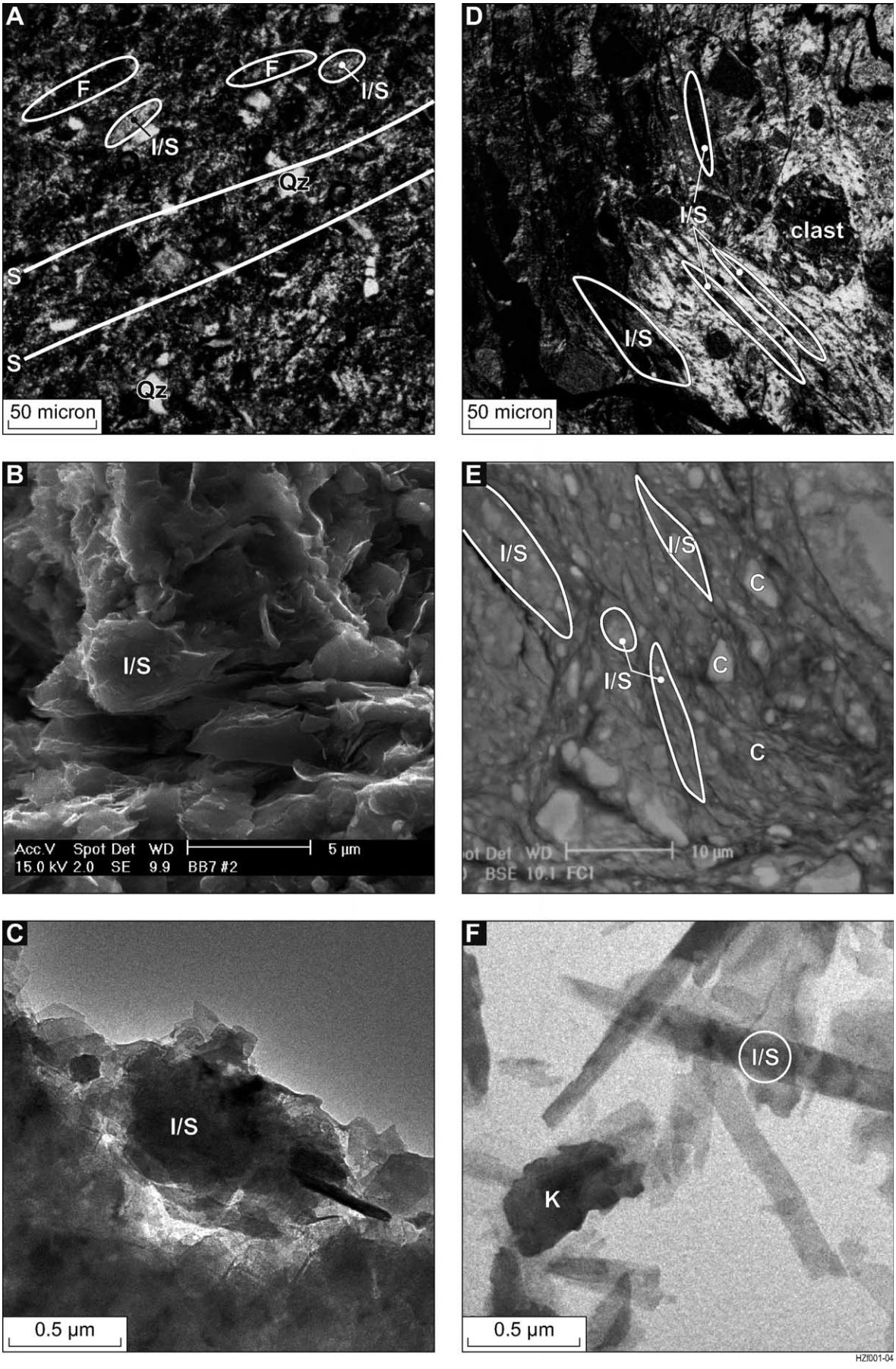
A
F
F
I/S
I/S
Qz
S
S
Qz
50 micron
D
I/S
clast
I/S
50 micron
B
I/S
Acc.V Spot Det WD 5 µm
15.0 kV 2.0 SE 9.9 BB7 #2
E
I/S
I/S
C
I/S
C
C
10 µm
BSE 10.1 FCI
C
I/S
0.5 µm
F
I/S
K
0.5 µm
HZI001-04

Table 3
Results of XRD analyses of 2–6, <2, <0.4 and <0.1 μm fractions

Specimen no.	Type	Mineralogy 2–6 m	2–6 μm % I in I/S	2–6 μm %2M$_1$	<2 μm % I in I/S	<0.5 μm %2M$_1$
(BB1)	Gouge	Q, (K), (I/S)	bd	15	~70	0
(BB2)	Gouge	Q, (I/S), (K)	69	10	bd	0
(BB3)	Tuff	Q, (I/S), (K)	60	15	bd	0
(BB4)	Gouge	Q, (I/S), (K)	70	13	bd	0
(BB5)	Gouge	Q, (I/S), (K)	~75	13	~80	0
(BB6)	Gouge	Q, (I/S), (K)	~70	~5	bd	0
(BB7)	Siltstone	Q, (I),C	bd	28	bd	0
(BB8)	Siltstone	Q, C, I	bd	~9	bd	0
(BB9)	Tuff	I/S,Q, (K)	77	~8	bd	0
(BB10)	Tuff	Q, I/S, K	bd	~11	bd	0
(BB11)	Gouge	Q, K, (I/S)	bd	17	bd	0

I—Illite, K—Kaolinite, C—Chlorite, I/S—illite–smectite ()—minor, bd—peaks poorly developed.

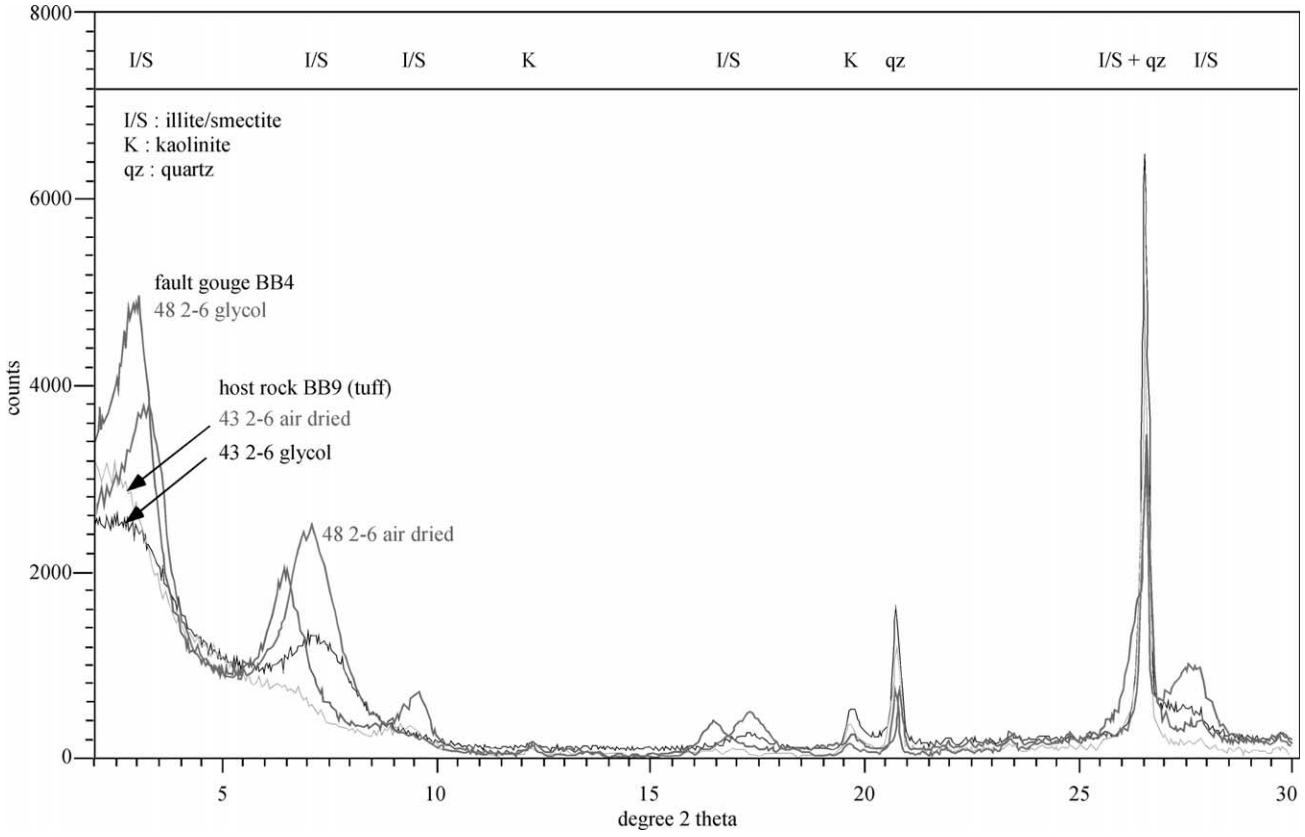

Fig. 3. Air-dried and glycolated XRD analyses of selected 2–6 μm size fraction from the gouge zone (BB4-43) and host rock (BB9-48).

Fig. 2. (A) Sample BB7. Photomicrograph of siltstone in damage zone showing scattered angular quartz grains in a matrix of fine grained illite–smectite (I/S) and disseminated wispy aggregates of coalified plant fragments (F) defining bedding (S). Cross polars (XPL). (B) SEM image of broken face of BB7 showing oriented crystallites of I/S. Note slightly irregular outline of crystallites. (C) TEM image of I/S detrital crystallites in BB7. (D) Sample BBI. Gouge from fault zone exhibiting subangular clasts of partly altered crystal tuff surrounded by oriented anastomosing aggregates of I/S. Typical I/S aggregates are pointed out by white dots. (E) SEM image of gouge showing orientated anastomosing I/S around angular fragments of tuff. C indicates a typical clast. (F) TEM image of separated authigenic elongated illite particles from sample BB1, K indicates a kaolinite particle.

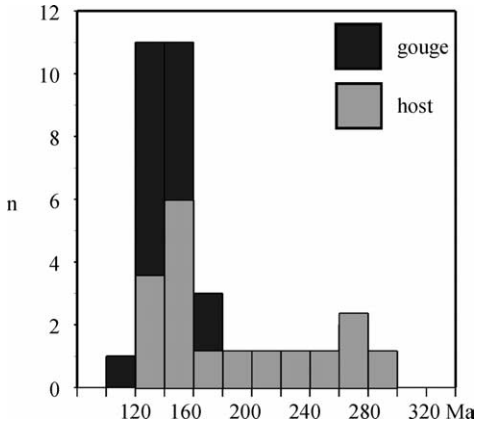

Fig. 4. Histogram of K–Ar results obtained from gouge zones and host rocks.

environments as the radiogenic isotope systematics of sedimentary rocks are complex due to the intimate mixture of detrital and authigenic origin often making it difficult to provide unambiguous ages.

6.2. Maximum ages

For neoformed illite, the finest separated particle size is derived from the ends of filamentous grains and should represent the most recently grown illite. Conversely, coarser sized fractions formed earlier during the illite formation process should yield older ages. However, there is also evidence that illite can recrystallize and coarsen by Ostwald ripening processes in some hydrothermal systems under conditions appropriate to the fault gouge zones considered here (Eberl and Środoń, 1988; Eberl et al., 1990). In reality, grain-size fractions of neoformed illite are mixtures of illite particles formed at different times during growth and this growth history is usually investigated by dating a range of different grain-size fractions. Illite in fault gouge is formed in a low-temperature environment where mineral reactions are governed by kinetics rather than equilibrium thermodynamics (Vrolijk and van der Pluijm, 1999). Small amounts of detrital contaminates for example detrital illite, K-feldspars and quartz, which can include radiogenic or excess Ar in fluid inclusions will influence the age of the mineral fraction. The resultant dates are therefore averages that we interpret as maximum ages. However, the maximum ages approximate the timing of cessation of illite growth (Lee et al., 1985).

6.3. Interpretation of results

The ages obtained from the fault gouges range between 119 and 172 Ma and fractions separated from host rock samples yield 120–281 Ma ages. A two-sided *t*-test (Robinson et al., 1993) was applied to investigate if the obtained <2 μm K–Ar ages from the host and gouge zone are statistically different, despite the fact that the test is statistically limited by purity of the sample material and the analytical uncertainty of the age determinations. The *t*-test suggests that the dates obtained from the gouge zone are statistically indistinguishable from those of the host rock. However, the dates obtained from the gouge zone samples (119–172 Ma) are overall younger and show a more restricted range compared with those obtained from the host rock samples (120–281 Ma; Fig. 4).

TEM investigations of the various fractions extracted from the host rocks show with exception of the <0.4 μm fraction from sample BB9, many particles with ragged edges are present. This suggests that the ages obtained have been affected by the presence of detrital muscovite. XRD analyses confirm this interpretation because the polytype $2M_1$ is present in varying proportions in the 2–6 μm fractions (Table 3). Further confirmation comes from the coarse fractions of samples BB7 and 8 (Table 2), which give ages (272–282 Ma) older than the age of the sequence (245–252 Ma; Roberts et al., 1996). In these samples, muscovite derived from the Devonian–Carboniferous accretion–subduction complex sequences, a major source of detritus for the Sydney Basin (Collins, 1991, and references therein), is probably present.

The wide age spread in the host rocks could also be due in part to an early diagenetic overprint, evidence for which is apparent in the finer fractions of siltstones BB7 and 8 (196–237 Ma; Table 2). Some of the spread in the ages obtained from the siltstones could be due to the presence of detrital illite but this cannot be a valid explanation for the range in ages shown by the tuffs. The age of 196 Ma determined from the <0.1 μm fraction of BB7 in the damage zone suggests that diagenetic illite may still have been forming at this time (Table 2). This would be a valid interpretation if the K–Ar systematics of BB7 had not been reset by fluids fluxing via fluid channels into this Late Permian sequence at the time movement occurred on the faults.

There is some evidence to support this as all fractions from the tuffs in the damage zone give relatively young K–Ar dates (121–146 Ma), which are similar to those obtained from the fault gouge (Table 2). The younger ages recorded in the tuffs suggest that ingress of fluids had occurred resulting in the neoformation of I/S or resetting of diagenetic I/S concomitant with the growth of I/S in the gouge. The more regular boundaries and larger size of the crystallites in the tuffs compared with those in the siltstones from the damage zone revealed by SEM studies, supports the former interpretation. It would appear that the tuffs took up the strain more readily than the siltstones creating channelways that allowed the migration of the fluids and subsequent growth of I/S.

The relationship of increasing K–Ar age with increasing grain size is illustrated in Figs. 5 and 6 and is consistent with increased contamination by detrital muscovite in the coarse fractions relative to the finer fractions. These results are

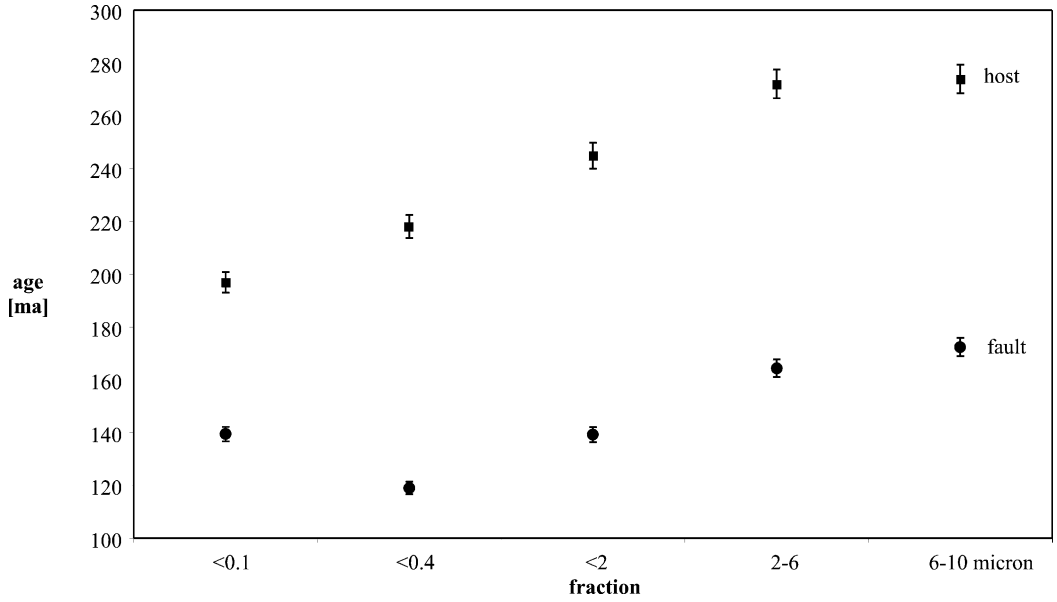

Fig. 5. K–Ar data for different size fractions obtained from fault gouge and host rocks.

similar to those obtained by Vrolijk and van der Pluijm (1999) from shales hosting thrust faults in the Canadian Rockies. The data suggest that the most reliable isotopic ages for neoformed illite are obtained from the finest size fractions (<0.1 μm) extracted from gouge and host rock samples. The relatively higher purity of the finest size fractions indicated by the XRD and TEM analyses is further evidence for the reliability of K–Ar dates obtained from the finest fractions. If this interpretation is correct then ages for <2 μm fractions range from 151 to 122 Ma (mean 135 Ma; $\sigma n-1=8.9$; $n=7$) and for <0.4 μm 119–121 Ma. It should be pointed out that an age of 139 Ma was obtained from the <0.1 μm fraction of BB1, older than the <0.4 μm fraction. This inverse age trend with increasing ages for the finest fraction may have been caused by contamination. An alternative explanation could be enrichment of illite nucleus particles or fundamental illite particles in the finest fraction as suggested by Clauer et al. (1997). These illite nucleus particles might be enriched within the finest <0.1 micron fraction and act as nuclei to grow larger illite particles (Nadeau, 1999). However, only one of our samples shows this inverse trend of older ages in finer fractions and it is not the general case. The true cause for this inverse age trend is still an open question. The variation in age with grain size in the finest fractions is still not large and changes little the interpretation of the ages obtained from the fault gouge.

7. Tectonic implications

The interpretation of the K–Ar ages obtained from the various fractions are summarized in Fig. 6 in relation to the diagenetic, sedimentary and tectonic history recorded by the rocks in the study area. The K–Ar ages (119–151 Ma; mean = 136 Ma) obtained from the <0.1, 0.4 and 2 μm fractions of the fault gouge provide the maximum age for the last slip event on the principle slip surfaces of the faults at Burwood Beach. In making this interpretation, we have assumed that new crystals of I/S grew synkinematically during the last phase of movement as a result of fluids fluxing into the core of the fault zones. Whether this interpretation is correct or not does not alter the significance of the ages determined from the finer fractions.

Further independent evidence supporting this interpretation can be drawn from dykes intruding NW–NNW-trending normal faults in the Newcastle area and south of the study area. They vary in age from 78 to 79 Ma (Norah Head and Fort Scratchley; unpubl. data Offler and Zwingmann) to 110 Ma (Fassifern location; Embleton et al., 1985). Thus movement on the normal faults like those at Burwood Beach is most likely older than 110 Ma. The Early Cretaceous dates obtained in this study are similar to those from the Bowen Basin (140–155 Ma; Uysal et al., 2001) and the Whitsunday Volcanic Province (WVP) central Queensland (95–132 Ma; Bryan et al., 1997). The 140–155 Ma dates according to Uysal et al. (2001), record a thermal event associated with rifting and widespread igneous activity that occurred prior to the break-up of Gondwana. The younger dates relate to volcanic activity in the WVP that forms part of a major meridionally orientated volcanic province extending 2500 km along the present eastern margin of Australia. The volcanism was associated with a rift system and Bryan et al. (1997) propose that this rift-related volcanic event brought about the dispersal of continental fragments of eastern Australian Gondwana. Our data confirm the studies of Bryan et al. (1997) and Uysal et al. (2001), and provide further evidence for the Early Cretaceous break-up of the eastern margin of Gondwana. The intraplate extension that occurred at this time led to the reactivation of N–S and NW dextral,

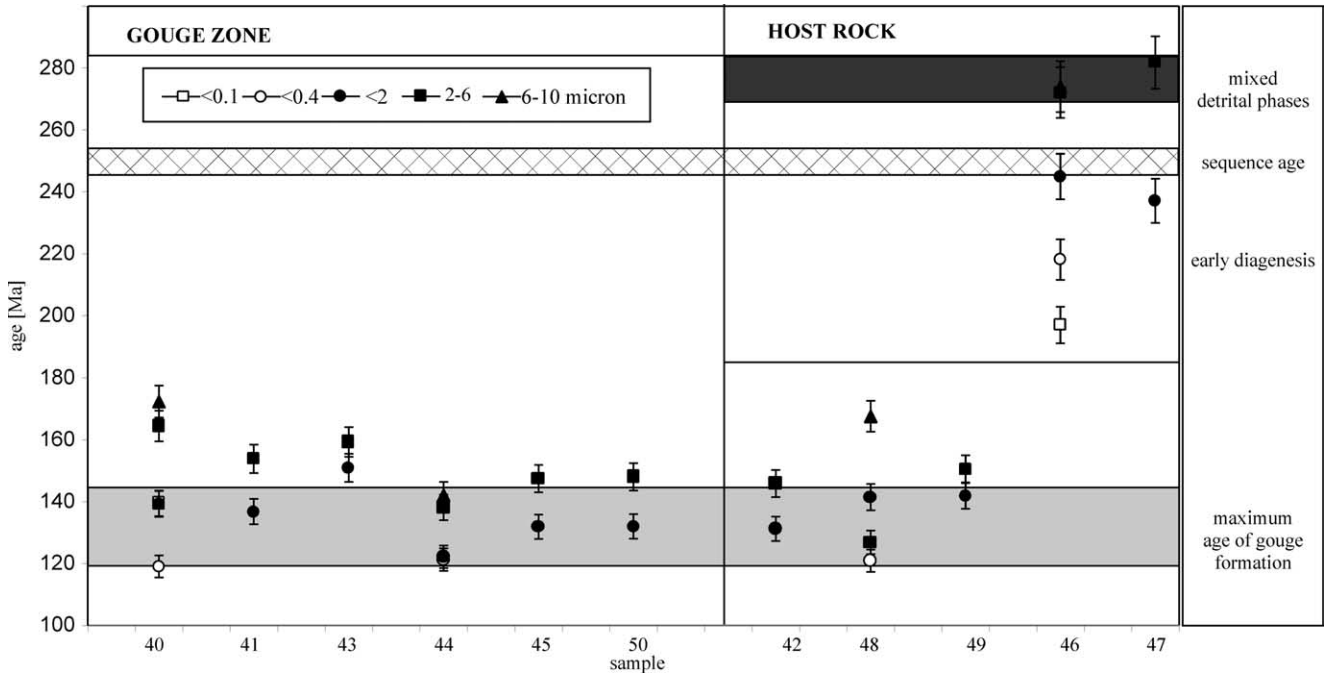

Fig. 6. Interpretation of K–Ar size fraction ages in relation to the diagenetic, sedimentary and tectonic history. Sequence age based on Roberts et al. (1996).

strike-slip faults that existed in the northern part of the Sydney Basin prior to this major event.

8. Conclusions

The 272–282 Ma K–Ar dates obtained from the coarse 2–6 μm fractions of the host rocks are older than the age of the sequence in which the samples, occur (245–252 Ma; Roberts et al., 1996). This suggests that detrital mica is present in these samples, consistent with petrographic and TEM studies. The younger ages of 197–237 Ma are thought to reflect the time at which the formation of diagenetic I/S occurred. By contrast, the <0.1, <0.4 and <2 μm ages (119–150 Ma) obtained from the fault gouge are thought to record the maximum age of the last slip event occurring on the faults, which we believe is related to Early Cretaceous rifting of the eastern margin of the Australian continent. Similar ages obtained from I/S in the finer fractions of the tuffs in the damage zone suggest fluids gained access to these rocks during this final movement. This study reports the first age data of synkinematic illite gouge material in Australia and highlights the potential and value of isotopic dating of synkinematic, neoformed illite in fault gouge to determine the timing of upper crustal deformation events.

Acknowledgements

Professor Ian McDougall, RSES, ANU, is thanked for his helpful advice during the set-up of the CSIRO Argon laboratory. Dr David Whitford's interest in low temperature diagenetic studies gave us the incentive to initiate this study. Andrew Todd and Andrew Bryce, CSIRO Petroleum, are thanked for technical assistance during the course of study. Tania Wilson was supported by a Faculty of Science and Mathematics Postgraduate Scholarship awarded to Stephen Cox. We thank Tom Blenkinsop from JSG for editorial assistance. Jim Dunlap and Tonguc Uysal are thanked for careful reviews, improving the original manuscript.

References

Barker, C.E., 1993. Calibration of a vitrinite reflectance geothermometer using peak temperature from fluid inclusions. American Chemical Society, Division of Geochemistry. 206th National Meeting, Chicago Abstract volume 19.

Blayden, I.D., 1971. On the structural evolution of the Macquarie Syncline, New South Wales. Ph.D. thesis. University of Newcastle (unpubl.).

Bonhomme, M.G., Thuizat, R., Pinault, Y., Clauer, N., Wendling, R., Winkler, R., 1975. Méthode de datation potassium–argon. Appareillage et technique. Strasbourg, 53pp.

Bryan, S.E., Constantine, A.E., Stephens, C.J., Ewart, A., Schoen, R.W., Parianos, J., 1997. Early Cretaceous volcano-sedimentary successions along the eastern Australian continental margin: implications for the break-up of eastern Gondwana. Earth and Planetary Science Letters 153, 85–102.

Choo, C.O., Chang, T.W., 2000. Characteristics of clay minerals in gouges of the Dongrae fault, Southeastern Korea, and implications for fault activity. Clays and Clay Minerals 48, 204–212.

Clauer, N., Chaudhuri, S., 1995. Clays and Crustal Cycles. Springer-Verlag, Heidelberg-New York.

Clauer, N., Srodon, J., Francu, J., Sucha, V., 1997. K–Ar dating of illite fundamental particles separated from illite/smectite. Clay Minerals 32, 181–196.

Collins, W.J., 1991. A reassessment of the "Hunter-Bowen Orogeny": Tectonic implications for the southern New England Fold Belt. Australian Journal of Earth Sciences 38, 409–423.

Diessel, C.F.K., 1975. Coalification trends in the Sydney basin, New South Wales, in: Campbell, K.S.W. (Ed.), Gondwana Geology. Australian National University Press, Canberra, pp. 295–309.

Diessel, C.F.K., 1992. Coal-Bearing Depositional Systems. Springer-Verlag.

Eberl, D.D., Środoń, J., 1988. Ostwald ripening and interparticle-diffraction effects for illite crystals. American Mineralogist 73, 1335–1345.

Eberl, D.D., Środoń, J., Kralik, M., Taylor, B.E., Peterman, Z.E., 1990. Ostwald ripening of clays and metamorphic minerals. Science 248, 474–477.

Embleton, B.J.J., Schmidt, P.W., Hamilton, L.H., Riley, G.H., 1985. Dating volcanism in the Sydney Basin, evidence from K–Ar ages and palaeomagnetism, in: Sutherland, F.L., Franklin, B.J., Waltho, A.E. (Eds.), Volcanism in Eastern Australia with Case Histories from New South Wales Geological Society of Australia, NSW Division, Publication, 1, pp. 59–72.

Emery, D., Robinson, A., 1993. Inorganic Geochemistry: Applications to Petroleum Geology. Blackwell, Oxford.

Hamilton, P.J., Kelley, S., Fallick, A.E., 1989. K–Ar dating of illite in hydrocarbon reservoirs. Clays and Clay Minerals 24, 215–231.

Hamilton, P.J., Giles, M.R., Ainsworth, P., 1992. K–Ar dating of illites Brent Group reservoirs: a regional perspective, in: Morton, A.C., Haszeldine, R.S., Giles, M.R., Brown, S. (Eds.), Geology of the Brent Group Geological Society Special Publication, 61, pp. 377–400.

Hunziker, J.C., Frey, M., Clauer, N., Dallmeyer, R.D., 1987. Reply to the comments on the evolution of illite to muscovite by J.R. Glasman. Contributions to Mineralogy and Petrology 96, 75–77.

Kralik, M., Klima, K., Riedmueller, G., 1987. Dating fault gouges. Nature 327, 315–317.

Lee, M., Aronson, J.L., Savin, S.M., 1985. K/Ar dating of Rotliegendes sandstone, Netherlands. American Association of Petroleum Geologists Bulletin 69, 1381–1385.

Liewig, N., Clauer, N., Sommer, F., 1987. Rb–Sr and K–Ar dating of clay diagenesis in Jurassic sandstone oil reservoirs, North Sea. American Association of Petroleum Geologists Bulletin 71, 1467–1474.

Lohe, E.M., McLennan, T.P.T., 1991. An overview of the structural fabrics of the Sydney Basin, and a comparison with the Bowen Basin. In: 25th Newcastle Symposium on "Advances in the Study of the Sydney Basin." University of Newcastle, NSW, Australia. Department of Geology, Publication 413, pp. 12–21.

Lohe, E.M., McLennan, T.P.T., Sullivan, T.D. Soole, K.P., Mallett, C.W., 1992. Sydney Basin – Geological Structure and Mining Conditions Assessment for Mine Planning. NERDDC Project No. 1239. Final Report. CISRO Division of Geomechanics, Institute of Minerals, Energy and Construction.

Lyons, J.B., Snellenberg, J., 1971. Dating faults. Geological Society of America Bulletin 82, 1749–1752.

McDougall, I., Roksandic, Z., 1974. Total fusion $^{40}Ar/^{39}Ar$ ages using HIFAR reactor. Journal of the Geological Society of Australia 21, 81–89.

Maxwell, S., 1990. Geochemical characterisation of dykes intruding the northern Sydney Basin, Australia. In: Parker, A.J., Rickwood, P.C., Tucker, D.H. (Eds.), Mafic Dykes and Emplacement Mechanisms. Balkema, Rotterdam, pp. 414–419.

Maxwell, D.T., Hower, J., 1967. High-grade diagenesis and low-grade metamorphism of illite in the Precambrian Belt Series. American Mineralogist 52, 843–857.

Merriman, R.J., Kemp, S.J., 1996. A basin maturity chart for clay minerals. Bulletin of the Mineralogical Society 111, 7–8.

Moore, D., Reynolds, R., 1989. X-Ray Diffraction and the Identification and Analysis of Clay Minerals. Oxford University Press, Oxford.

Nadeau, P.H., 1999. Fundamental particles: an informal history. Clay Minerals 34, 185–191.

Pevear, D.R., Vrolijk, P.J., Longstaffe, F.J., 1997. Timing of Moab Fault displacement and fluid movement integrated with burial history using radiogenic and stable isotopes. In: GEOFLUIDS II '97 Extended Abstracts, pp. 42–45.

van der Pluijm, B.A., Hall, M., Vrolijk, P., Pevear, D.R., Covey, M., 2001. The dating of shallow faults in the earth's crust. Nature 412, 172–174.

Roberts, J., Claoue-Long, J.C., Foster, C.B., 1996. SHRIMP zircon dating of the Permian System of eastern Australia. Australian Journal of Earth Sciences 43, 401–421.

Robinson, A.G., Coleman, M.L., Gluyas, J.G., 1993. The age of illite cement growth, Village Fields area, Southern North Sea: evidence from K–Ar ages and $^{18}O/^{16}O$ ratios. American Association of Petroleum Geologists Bulletin 77, 69–80.

Steiger, R.H., Jäger, E., 1976. Subcommission on geochronology: convention on the use of decay constants in geo- and cosmochronology. Earth and Planetary Science Letters 36, 359–362.

Uysal, T., Golding, S.D., Thiede, D.S., 2001. K–Ar and Rb–Sr dating of authigenic illite–smectite in Late Permian coal measures, Queensland, Australia: implication for thermal history. Chemical Geology 171, 195–211.

Vrolijk, P., van der Pluijm, B.A., 1999. Clay gouge. Journal of Structural Geology 21, 1039–1048.

Wilson, T., Offler, R., Cox, S.F., 2000. Interpretation of brittle microstructures. 15th Australian Geological Convention, Sydney, July 2000. Geological Society of Australia Abstracts No. 59, p. 545.